

OPTIMUM DESIGN OF SWEPT-FORWARD
HIGH-ASPECT-RATIO GRAPHITE-EPOXY WINGS

M. J. Stuart
NASA Langley Research Center
Hampton, Virginia

R. T. Haftka
Virginia Polytechnic Institute and State University
Blacksburg, Virginia

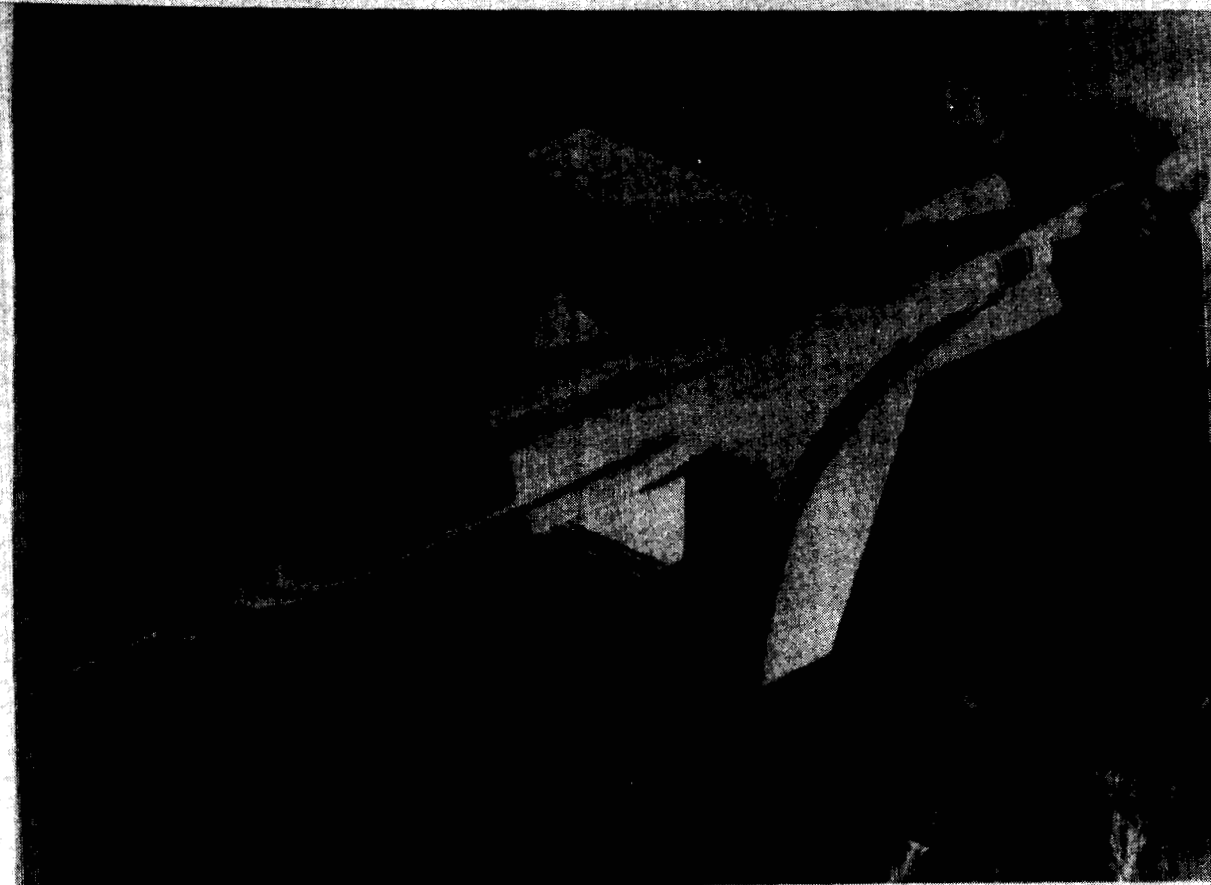
R. L. Campbell
NASA Langley Research Center
Hampton, Virginia

INTRODUCTION

The efficiency of aerospace structures is evaluated by many criteria that may include performance, structural weight, and cost. Anisotropic composite materials have characteristics that are useful for the design of innovative aerospace structures. These materials are well-known for their high strength- and stiffness-to-weight ratios. Lightweight composite structures also can have unique response characteristics that enable the design of innovative structural concepts. An example of these characteristics is the beneficial bending/twisting coupling response of the graphite-epoxy wing skins for the swept-forward X-29 wing (see Figure 1). Moreover, recent advances in materials and processing technologies indicate that composite structures may be fabricated for a lower cost when compared to similar metallic structures. Additional research is needed to exploit the unique characteristics of composite structures to obtain structurally efficient, cost-effective designs.

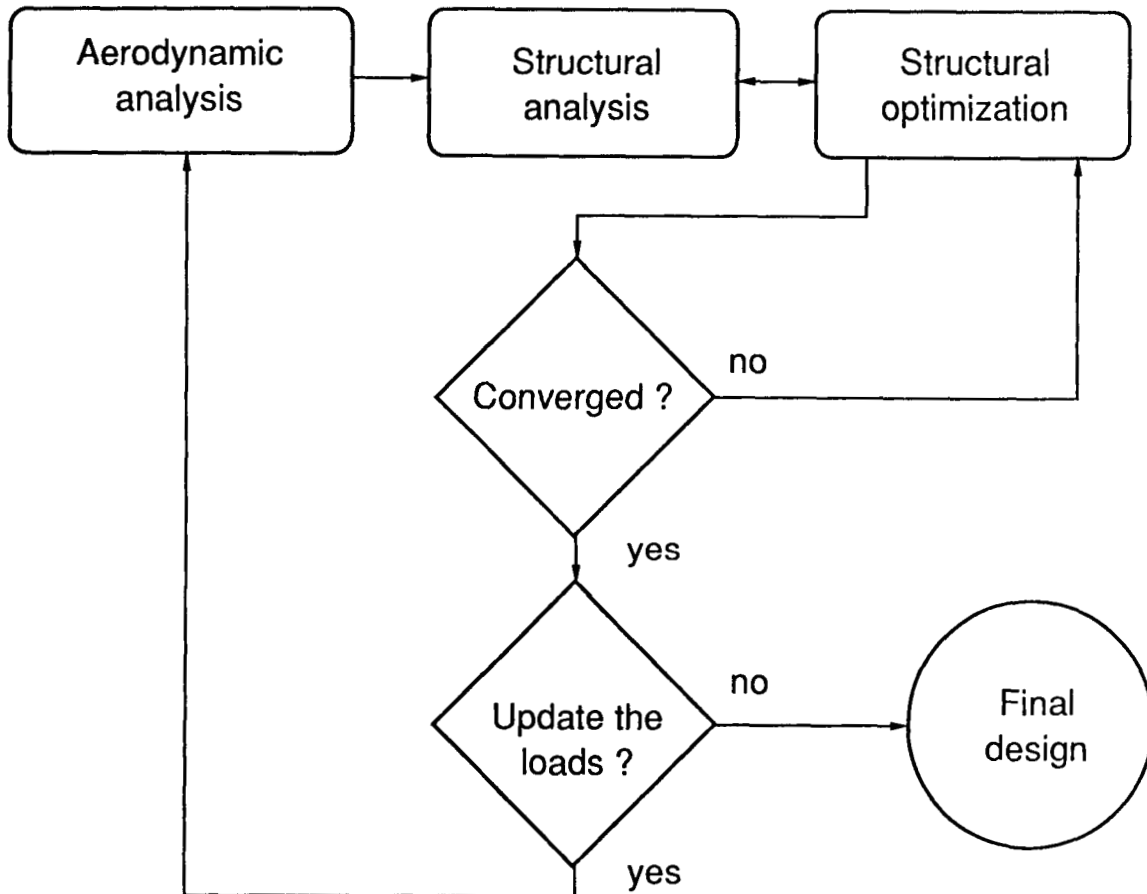
This paper describes an analytical investigation of a swept-forward high-aspect-ratio graphite-epoxy transport wing. The objectives of this investigation were to illustrate an effective usage of the unique properties of composite materials by exploiting material tailoring and to demonstrate an integrated multidisciplinary approach for conducting this investigation.

X-29 ADVANCED TECHNOLOGY DEMONSTRATOR



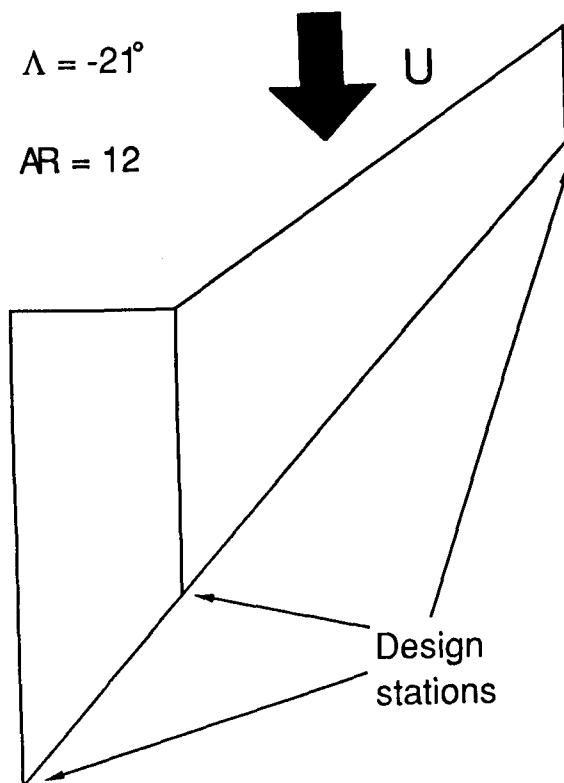
AN INTEGRATED APPROACH TO WING DESIGN

The integrated multidisciplinary procedure used in this investigation is illustrated in Figure 2. This procedure consists of an aerodynamic analysis, a structural analysis, and a structural optimization. The aerodynamic analysis of the wing configuration includes aeroelastic corrections to account for structural deformations and produces the wing loading. The structural analysis uses the wing loading to calculate stresses, strains, and deformations for the internal wing structure. The structural optimization compares these stresses, strains, and deformations against design constraints and perturbs the internal wing structure to obtain a minimum weight structural configuration that satisfies the design constraints. The optimized configuration is input to the aerodynamic analysis to update the wing loading, and the entire procedure is repeated to obtain a second optimized configuration. The second configuration is used as the final design.



FORWARD SWEPT WING GEOMETRY

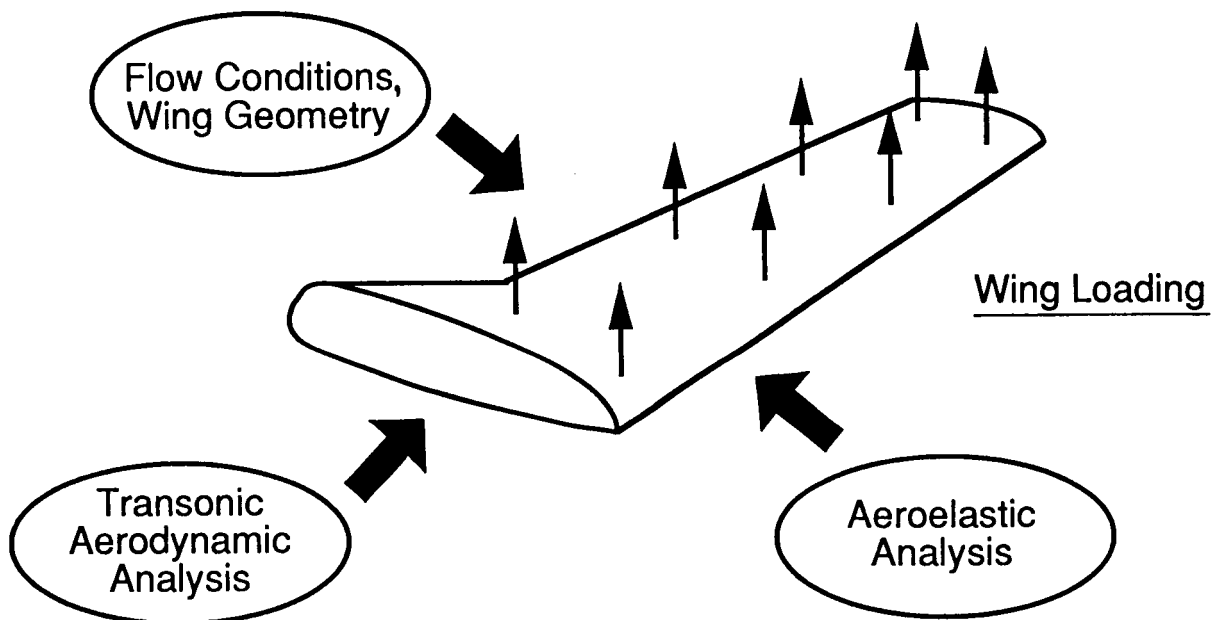
The wing geometry selected for this investigation is shown in Figure 3. The primary goal for the aerodynamic design of this wing was to reduce drag by natural laminar flow (NLF). Forward sweep appears to be advantageous for obtaining NLF since the flow along the leading edge of the wing would not be contaminated by the turbulent boundary layer from the fuselage. A moderate leading-edge sweep, -21° , was chosen in order to reduce the possibility of boundary layer transition due to cross-flow instabilities. The aspect ratio for this wing is 12. The flight conditions at the cruise design point were a Mach number of 0.78 and a lift coefficient of 0.55 at an altitude of 39,000 ft. The airflow is indicated by U on the figure. A parametric study of the effect of planform variations on wing shock strength and location was made at these flight conditions using the TAWFIVE full-potential wing-body computer code (ref. 1). The sweep of the leading and trailing edges of the wing from the root to about forty percent of the semispan was varied in an effort to reduce the shock strength over the inboard part of the wing. For the configurations examined, the best performance resulted from having a constant trailing-edge sweep for the entire wing and an unswept leading edge for the inboard portion of the wing. Airfoil geometry is determined using the pressure distributions at the three design stations indicated on the figure.



- Drag reduction through natural laminar flow
- Cruise design point:
 $M=0.78$, $C_L=0.55$, alt=39,000 ft
- TAWFIVE for planform design
 - full-potential wing-body code
 - reduce shock strength inboard

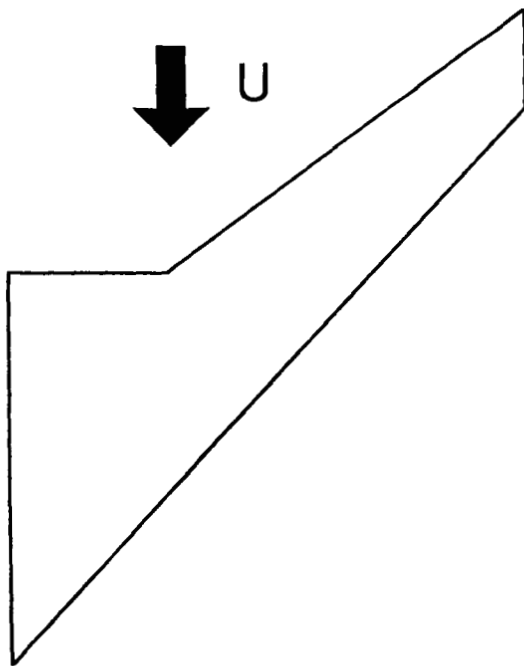
TRANSONIC AEROELASTIC PROGRAM SYSTEM (TAPS)

The aerodynamic loads were calculated using the Transonic Aeroelastic Program System (TAPS, ref. 2), and this system is illustrated schematically in Figure 4. The two main components of TAPS are an aerodynamic analysis code and an aeroelastic module. The TAWFIVE transonic wing-body code (ref. 1) was used for the aerodynamic calculations in this study. An initial aerodynamic analysis is made using specified flow conditions and the unloaded wing geometry. The resulting wing pressure coefficients are interpolated to the structural node locations, converted to lifting pressures using the free-stream dynamic pressure, and multiplied by input nodal areas to yield an array of nodal forces. This array is then multiplied by the structural flexibility matrix to obtain the vertical deflection at each node location. These static aeroelastic deflections are interpolated back to the wing planform locations needed for the aerodynamic analysis code. The deflected wing geometry is then analyzed in TAWFIVE to get a new estimate of the wing loading. The TAPS method updates the wing loading and deflections in this manner for a user-specified number of cycles. The calculations in this study were made using three aerodynamic-structural iterations.



GLOBAL STRUCTURAL OPTIMIZATION FOR ADVANCED CONCEPT WINGBOX

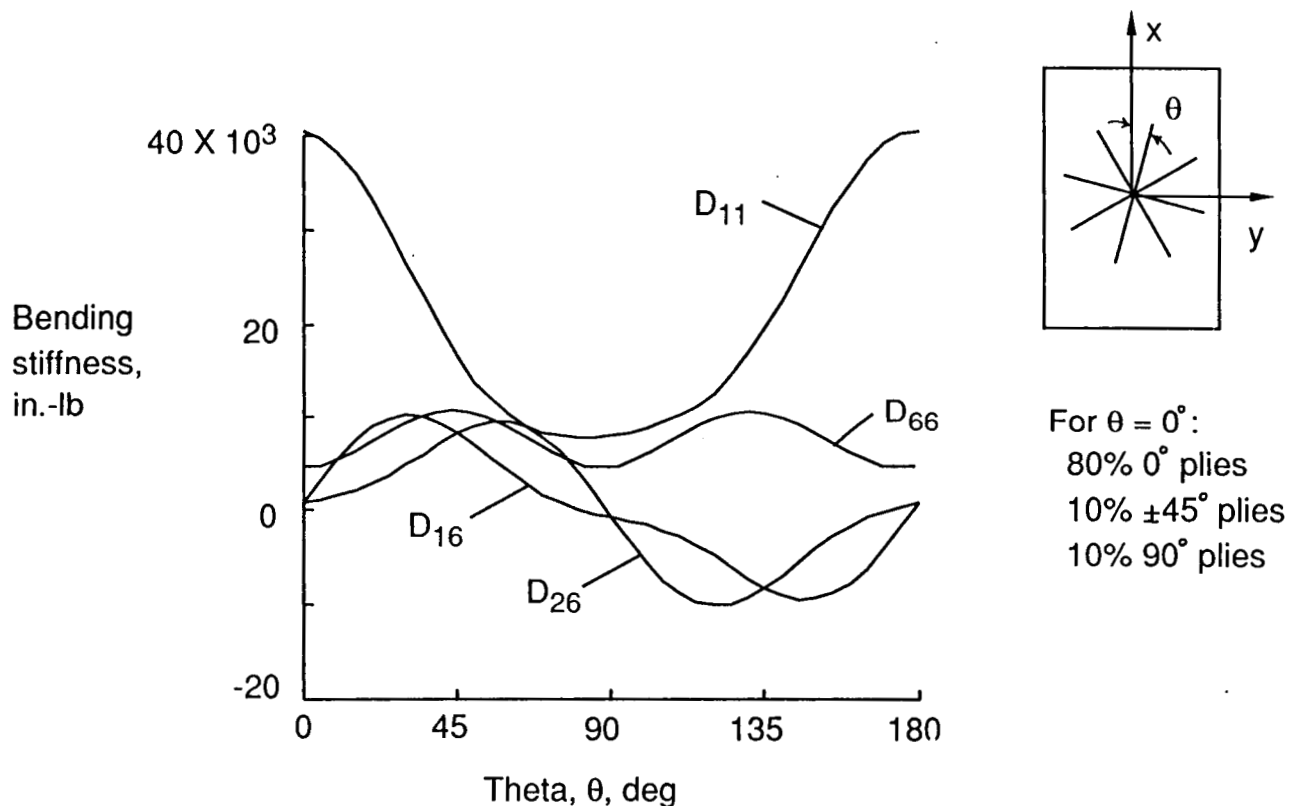
The loading conditions, design variables, and parameters for this high-aspect-ratio wing configuration are shown in Figure 5. Two loading conditions that significantly affect the response of a high-aspect-ratio wing were considered: a 2.5-g maneuver condition; and a gust-up condition. The 2.5-g maneuver condition was simulated by increasing the dynamic pressure at the cruise Mach number and angle of attack. The gust-up condition was simulated by modifying the angle of attack at the cruise Mach number. The loads obtained for these two conditions were multiplied by a 1.5 factor of safety. The graphite-epoxy wingbox consisted of orthotropic cover panel laminates, quasi-isotropic rib web laminates, and quasi-isotropic spar cap and spar web laminates. The design variables selected for optimization of the graphite-epoxy wingbox were material orientations for the cover panels (as determined by the laminate's 0° direction), ply thicknesses for the cover panel laminates, and cross-sectional areas for the spar caps. The parameters that were varied for this investigation were the number of spars, the number of ribs, the rib orientation with respect to the leading edge spar, and the graphite-epoxy material properties.



- Loading conditions
2.5 G maneuver
gust up
- Design variables
material orientations
ply thicknesses
spar cap areas
- Parameters
number of spars
number of ribs
rib orientation
material properties

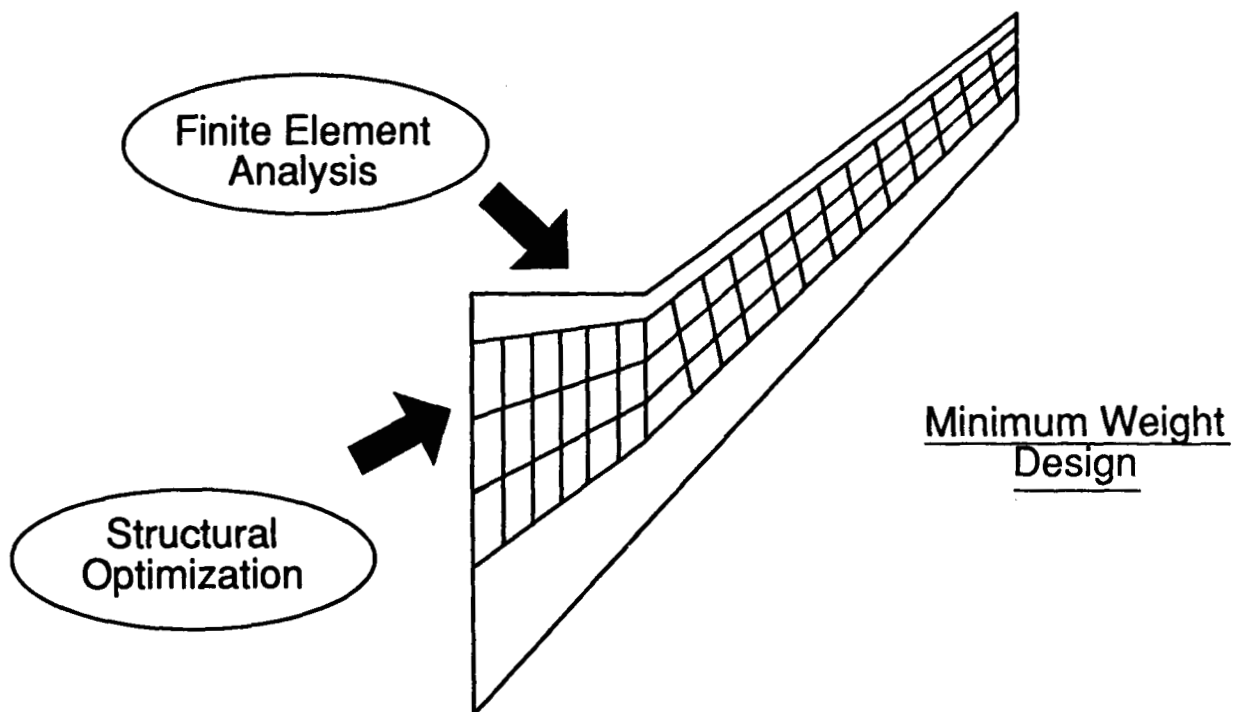
BENDING STIFFNESS VARIATIONS FOR AN ORTHOTROPIC LAMINATE

The tailorability of an orthotropic graphite-epoxy laminate is illustrated in Figure 6. The laminate described on the figure has 80 percent 0° plies, 10 percent $\pm 45^\circ$ plies, and 10 percent 90° plies when the 0° direction is parallel to the x-axis ($\theta=0^\circ$). The bending/torsional stiffnesses for this laminate change dramatically as the angle θ between the x-axis and the 0° direction varies from 0° to 180° . For example, the D_{11} bending stiffness value is more than an order of magnitude greater than all other values for $\theta=0^\circ$ but is approximately the same as the D_{26} and D_{66} bending stiffness values for $\theta=70^\circ$. Also, the bending-torsion coupling term D_{16} critical for a forward-swept wing changes sign as θ is varied. In the present study, the wing tip was constrained to have zero twist deformation by the structural optimization module to guard against unfavorable bending-torsion coupling leading to aeroelastic instabilities. This constraint results in a selection of θ that uses anisotropy to cancel the unfavorable geometrical coupling inherent in a forward-swept wing.



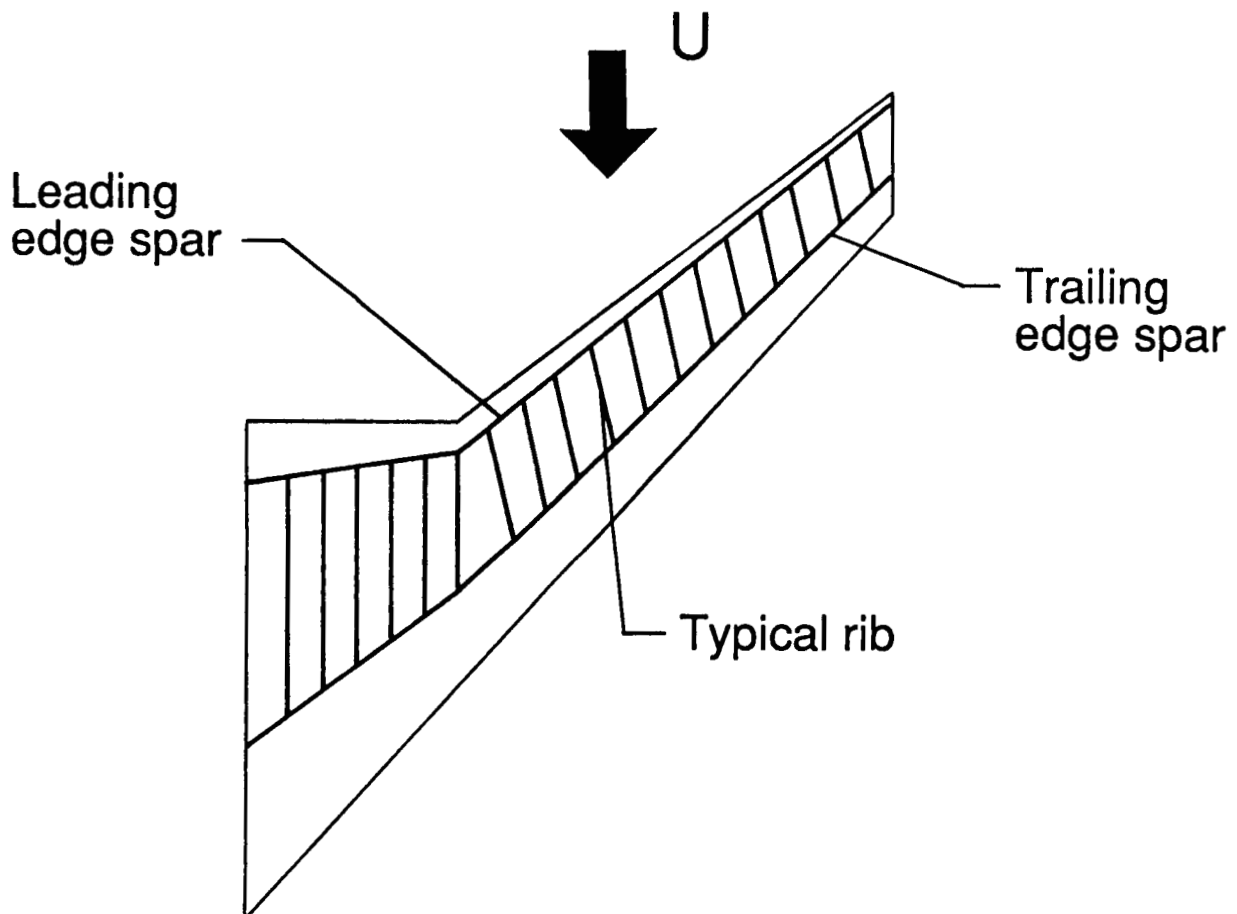
WING DESIGN OPTIMIZATION WITH AEROELASTIC CONSTRAINTS (WIDOWAC)

The structural optimization was carried out with a modified version of the WIDOWAC program (ref. 3), and this program is shown schematically in Figure 7. The program employs a built-up finite-element model of the wing consisting of membrane quadrilateral elements for cover panels and combinations of rod elements and shear elements for ribs and spars. A quadratic extended interior penalty function is used for the optimization. The structure was optimized subject to maximum strain constraints (e.g., $|\epsilon| \leq 0.006$, $|\gamma| \leq 0.010$), minimum gage constraints (ply thickness ≥ 0.0074 in.), and side constraints that limited the percentage of ply thickness for any orientation to no less than 10 percent of the laminate thickness. To guard against aeroelastic instabilities two stiffness constraints were applied. The first stiffness constraint required a minimum torsional stiffness for the wing, and the second stiffness constraint mandated a zero or negative twist angle at the wing tip when the wing is subjected to each design load. The WIDOWAC program was used to obtain minimum weight designs for this wing configuration.



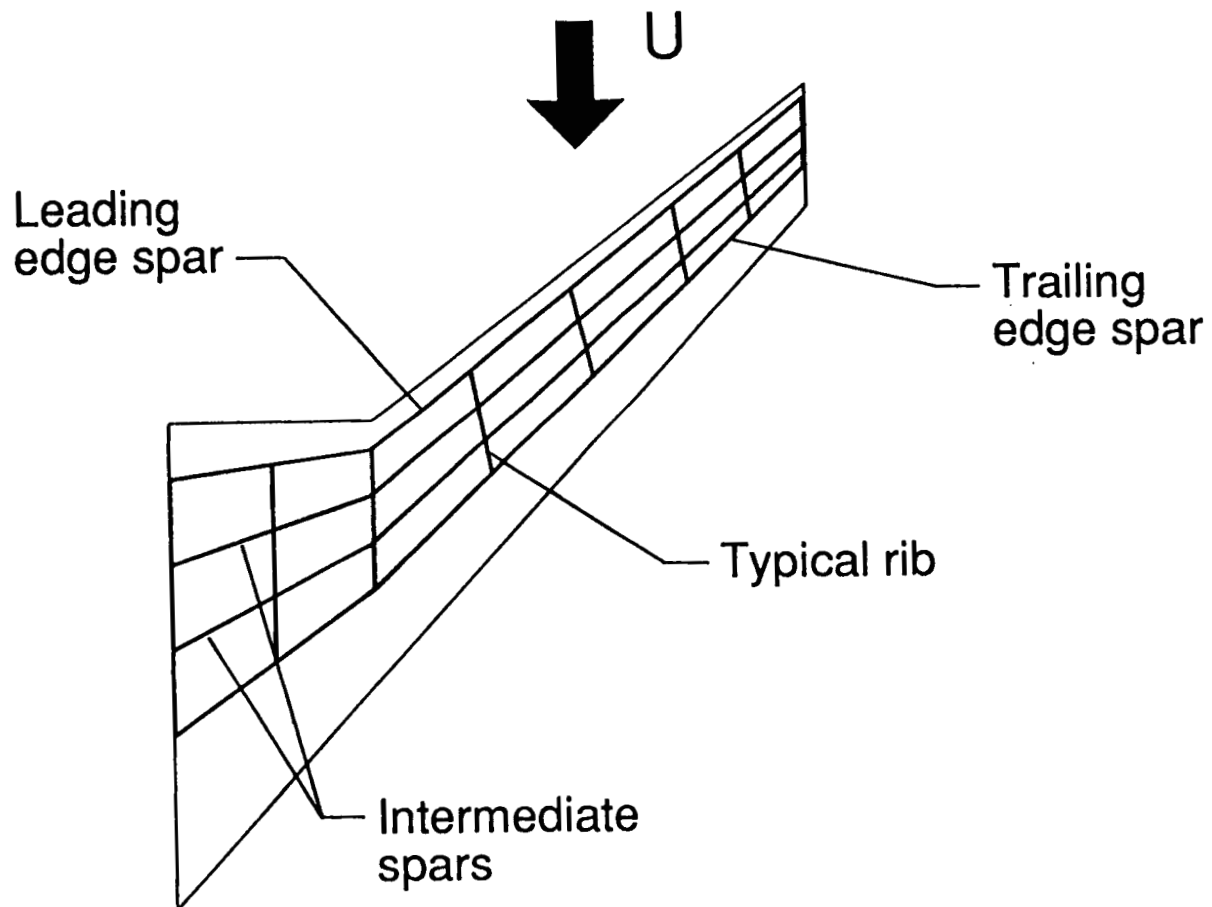
2-SPAR MODEL

Three wingbox models were used to investigate the effects of wingbox configuration on the configuration weight. These models are referred to as the 2-spar model, the 4-spar model, and the multi-spar/multi-rib model. These models were used to obtain results for configurations fabricated using either a state-of-the-art damage-tolerant graphite-epoxy material or an improved graphite-epoxy material. The state-of-the-art graphite-epoxy material is referred to as the standard material. The improved material is not currently available but is assumed to have stiffness and strength properties that are 20% greater than the respective properties for the standard material. The 2-spar model is illustrated in Figure 8. This model is used to represent a wingbox configuration having leading and trailing edge spars and having ribs spaced 30 in. apart. The configuration has a total of twenty ribs. This configuration is typical of current wingbox configurations for transport aircraft.



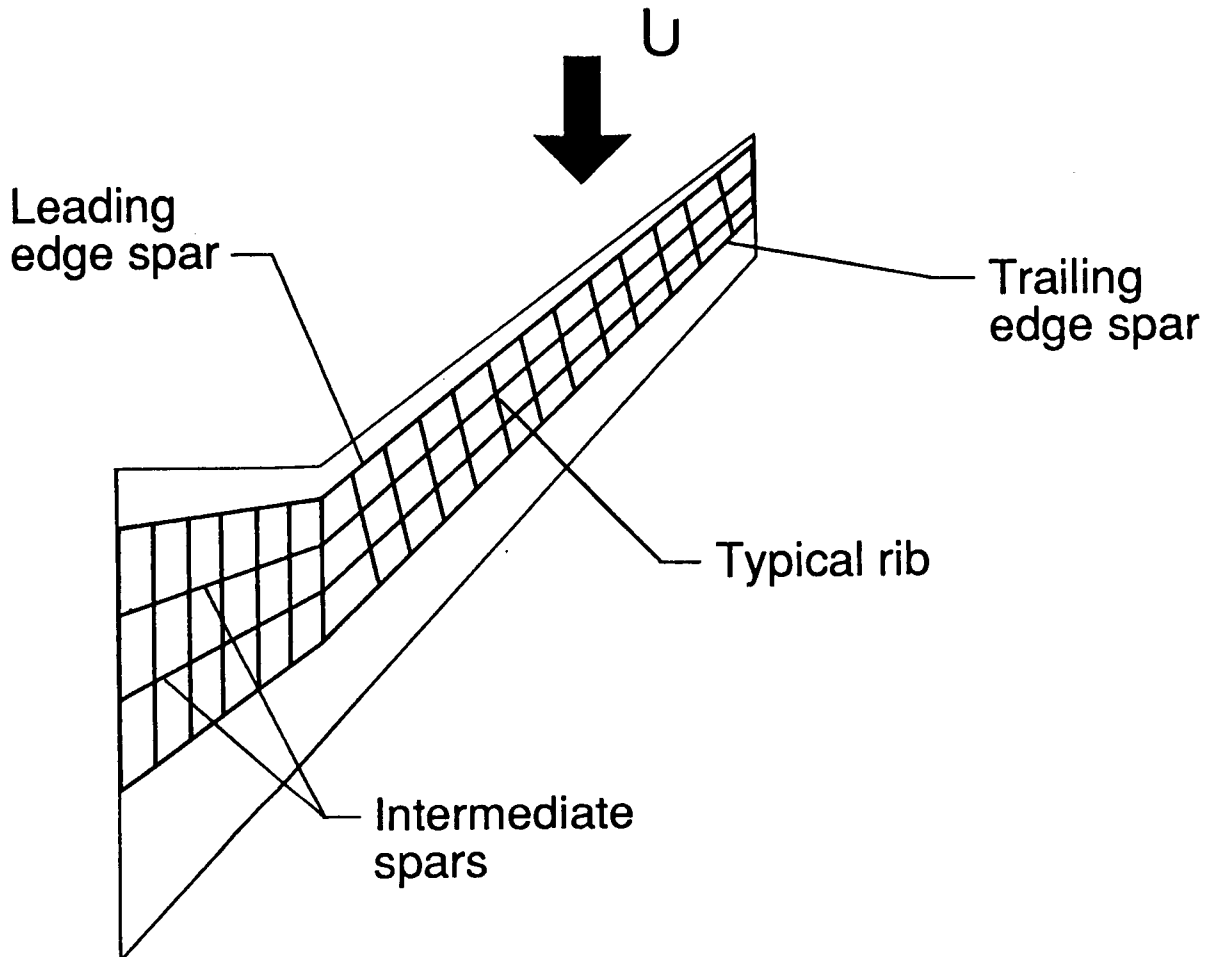
4-SPAR MODEL

The 4-spar wingbox model is shown in Figure 9. This model is used to represent a wingbox configuration having leading and trailing edge spars as well as two interior spars. The number of ribs for this model is minimized to seven.



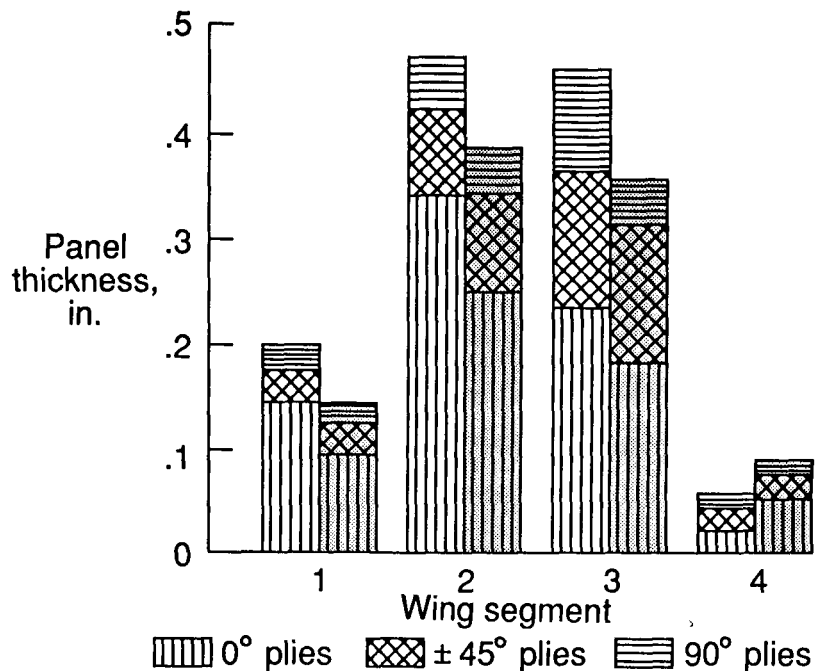
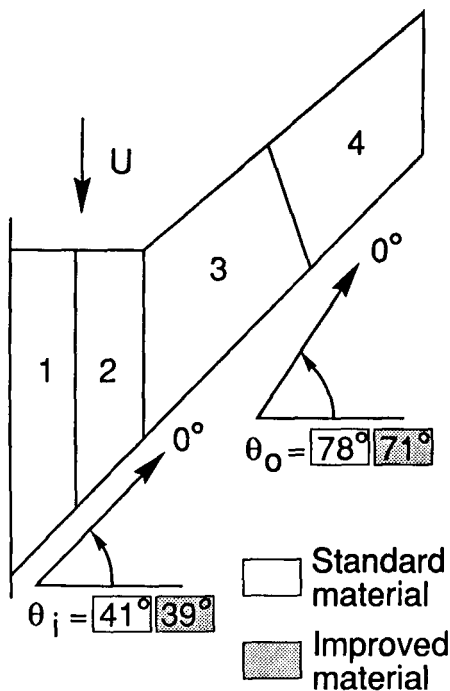
MULTI-SPAR/MULTI-RIB (MR/MS) MODEL

The multi-spar/multi-rib (MS/MR) model is shown in Figure 10. The MS/MR model is a combination of the 2-spar and the 4-spar models. The MS/MR model has a leading edge spar, a trailing edge spar, two interior spars, and ribs spaced 30 in. apart.



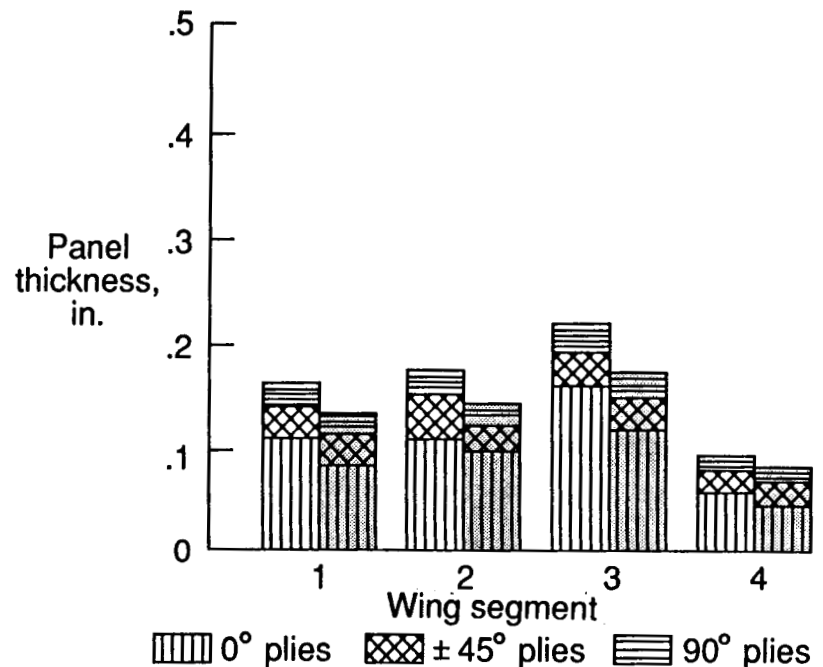
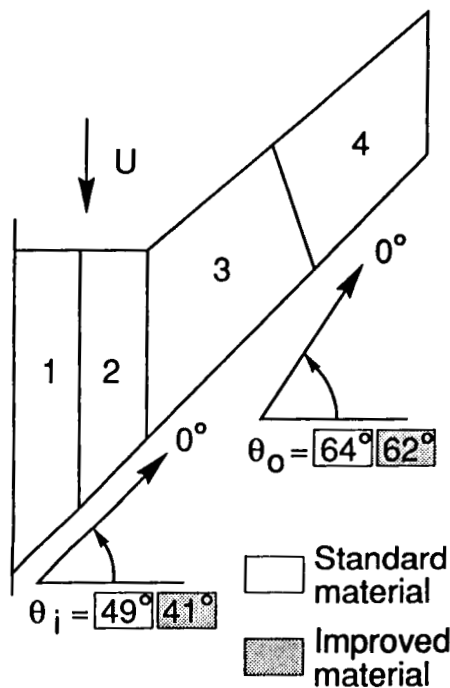
OPTIMIZED THICKNESS DISTRIBUTION FOR TOP COVER PANEL OF 2-SPAR WINGBOX

The wingbox models were used to determine cover panel thicknesses for the four regions of the wingbox, and results obtained using the 2-spar are shown in Figure 11. The wingbox regions are illustrated on the left side of the figure, and the top cover panel thicknesses for these regions are illustrated on the right side of the figure. The inboard orientation angle θ_i is the 0° material direction for regions 1 and 2; the outboard orientation angle θ_o is the 0° material direction for regions 3 and 4. Results for a configuration that uses the standard material are unshaded on the figure, and results for a configuration that uses the improved material are shaded on the figure. The values of θ_i and θ_o for both the standard and the improved materials indicate that significant bending-twisting coupling occurs for this configuration. The panel thickness results show regions 2 and 3 to be much thicker than regions 1 and 4, indicating that the region 2-3 interface is heavily loaded. Results for a configuration fabricated from an improved material show a 20 percent decrease in thickness that corresponds to the 20 percent increase in stiffness and strength properties.



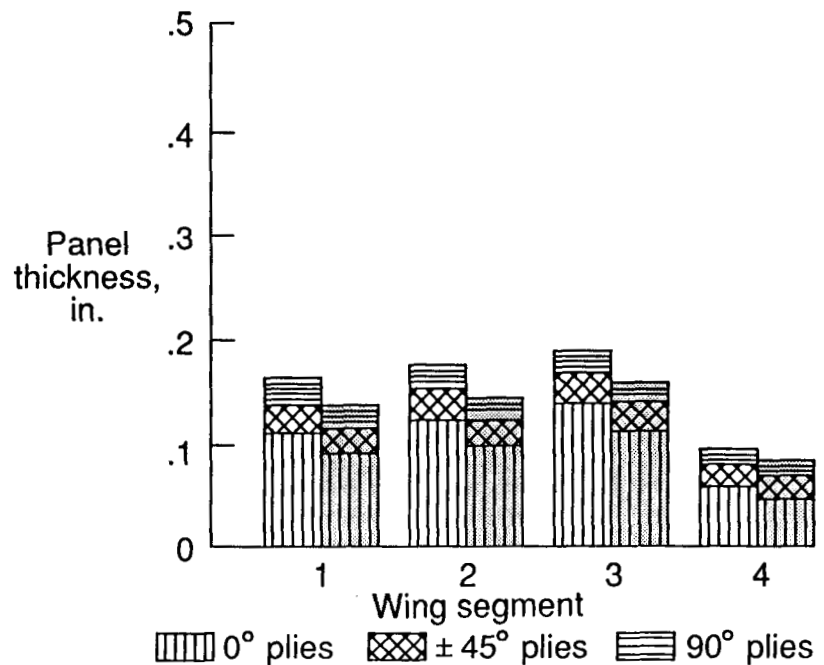
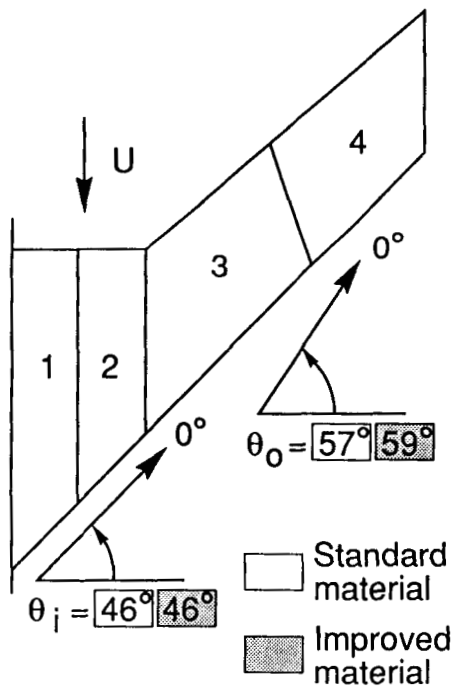
OPTIMIZED THICKNESS DISTRIBUTION FOR TOP COVER PANEL OF 4-SPAR WINGBOX

Results obtained using the 4-spar model are shown in Figure 12. The thicknesses for regions 1, 2, and 3 obtained using the 4-spar model are significantly less (e.g., 63 percent less, region 2) than the respective thicknesses obtained using the 2-spar model. Also, the percentages of $\pm 45^\circ$ and of 90° plies determined using the 4-spar model are approximately equal to the 10 percent minimum. These results for individual ply thicknesses suggest that the 4-spar configuration combines aeroelastic tailoring with an efficient internal structure to achieve a lightweight feasible design. Results for a configuration fabricated from an improved material show a 20 percent decrease in thickness that corresponds to the 20 percent increase in stiffness and strength properties.



OPTIMIZED THICKNESS DISTRIBUTION FOR TOP COVER PANEL OF MULTI-SPAR/MULTI-RIB WINGBOX

Results obtained using the multi-spar/multi-rib (MS/MR) model are shown in Figure 13. The standard material or improved material thicknesses obtained using the MS/MR model are approximately the same as the respective thicknesses obtained using the 4-spar model. The MS/MR results suggest that the MS/MR configuration can be used to achieve lightweight feasible designs. However, the MS/MR configuration may be much more costly than the 4-spar configuration as determined by configuration part count. The MS/MR configuration has the same number of spars but has many more ribs than the 4-spar configuration. Typically, configuration cost increases with increasing part count.



ORIENTED-RIB RESULTS: 2.5 G MANEUVER

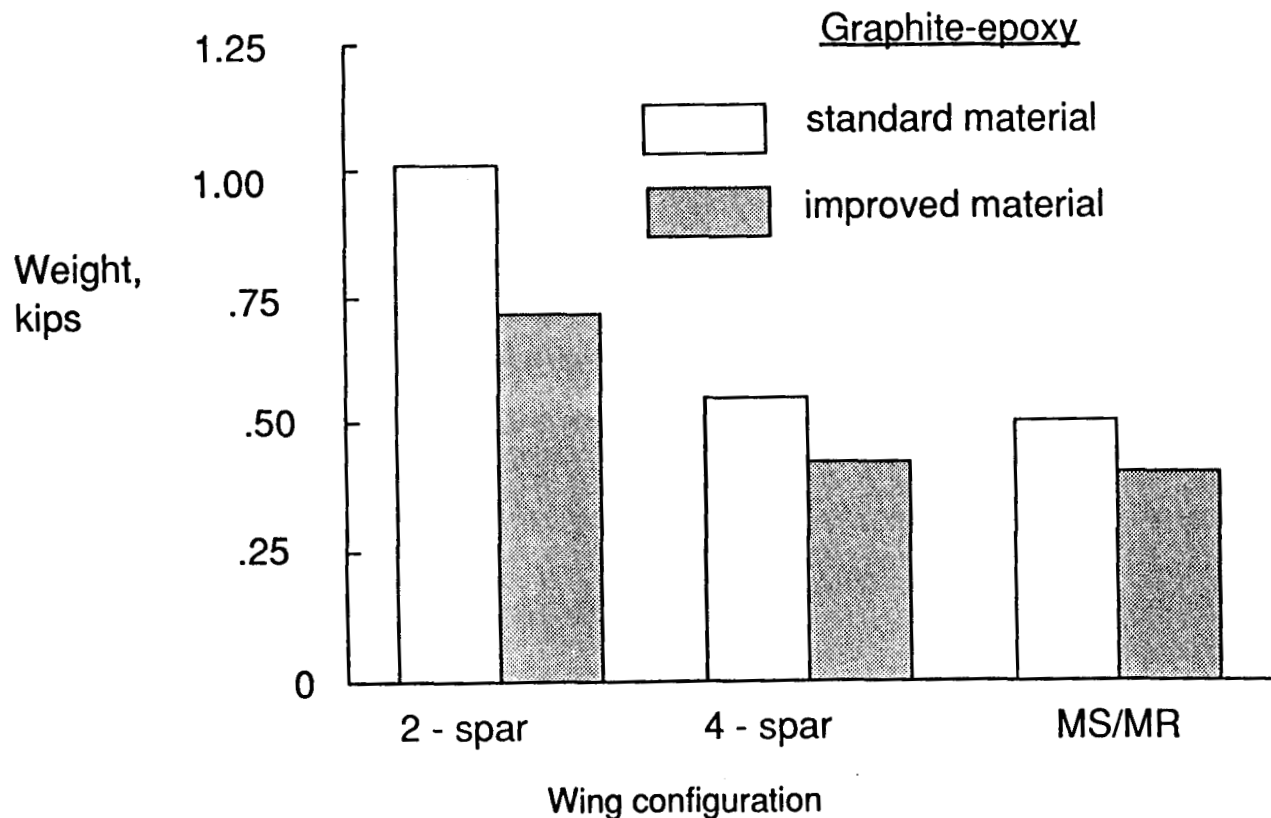
The effect of rib angle on the wingbox configuration weight was investigated by changing the angle between ribs and the leading edge spar from 90° to 80° and then to 100°. Unfortunately, these changes apparently led to aeroelastic divergence instability which was evidenced by the high values for the tip twist angle after three aeroelastic iterations (Figure 14). A non-diverging design for the two rib-orientation configurations would have been possible if the aeroelastic analysis were a part of the optimization process. However, the extreme sensitivity to rib angles illustrates an inadequacy inherent in present deterministic design procedures. These procedures specify safety margins in terms of the applied loads. However, the present results indicate that a structure can have adequate load-based safety margins but lack a margin of safety with respect to small changes in the structure. These small changes may actually occur due to manufacturing tolerances and aging. A reliability-based design procedure with constraints on failure probabilities may avoid the inadequacy inherent in deterministic design procedures.

Orientation angle, deg	Tip Twist, deg	
	standard material	improved material
80	23.3	16.2
100	24.7	11.5

- Present model indicates divergence
- Model extremely sensitive
- Deterministic-based designs vs. reliability-based designs

OPTIMIZED WEIGHT FOR WINGBOX

The optimized weight for the three wingbox configurations is shown in Figure 15. Results are presented for configurations fabricated with the standard material and for configurations fabricated with the improved material. The results show that the 2-spar configuration is the heaviest of the configurations studied. This configuration satisfies the design constraints using thick tailored cover panels. The 4-spar and the MS/MR configurations are approximately 45 percent and 50 percent lighter, respectively, than the 2-spar configuration. The 4-spar and the MS/MR configurations combine an efficient internal structure with tailored cover panels to achieve feasible lightweight designs. The 4-spar configuration appears to be the best configuration of the configurations studied. The 4-spar configuration has approximately the same weight as the MS/MR configuration, but the 4-spar configuration is much simpler than the MS/MR configuration.



CONCLUDING REMARKS

An analytical investigation of a swept-forward high-aspect-ratio graphite-epoxy transport wing has been described. An integrated multidisciplinary procedure was discussed that included an aerodynamic analysis, a structural analysis, and a structural optimization. This procedure was used to study 2-spar, 4-spar, and multi-spar/multi-rib (MS/MR) wingbox configurations. Results were obtained for configuration fabricated from either a state-of-the-art damage-tolerant graphite-epoxy material or an improved graphite-epoxy material. The improved material had stiffnesses and strengths that were 20 percent greater than the corresponding properties for the state-of-the-art material.

The integrated procedure demonstrated the tailorability of composite structures for advanced concept wingbox configurations. Improved materials, tailorability, and efficient internal structure led to lightweight feasible designs. The designs appeared to be very sensitive to rib orientation. Ribs oriented at 80° or at 100° to the leading edge spar may lead to an aeroelastic divergence instability. The 4-spar and MS/MR configurations had approximately the same weight and were significantly lighter than the 2-spar configuration. The 4-spar configuration was the best of the configurations considered because the 4-spar configuration is both lightweight and simple.

REFERENCES

1. Melson, N. D.; and Streett, C. L.: TAWFIVE: A User's Guide. NASA TM-84619, September 1983.
2. Campbell, R. L.: Calculated Effects of Varying Reynolds Number and Dynamic Pressure on Flexible Wings at Transonic Speeds. Recent Experiences in Multidisciplinary Analysis and Optimization, NASA CP 2327, 1984, pp. 309-327.
3. Haftka, Rafael T; and Starnes, James H., Jr.: WIDOWAC (Wing Design Optimization with Aeroelastic Constraints): Program Manual. NASA TM X-3071, October 1974.